Brownian motion of a colloidal particle immersed in a polymeric solution near a rigid wall

B. L. Arenas-Gómez and M. D. Carbajal-Tinoco

Departamento de Física, Centro de Investigación y de Estudios Avanzados del IPN,
Apartado Postal 14-740, México, 07000 D.F., Mexico,
e-mail: mdct@fis.cinvestav.mx

By using three-dimensional digital video microscopy (DVM-3D), we study the displacement of a Brownian particle immersed in a polymeric solution located near a rigid wall. The technique takes advantage of the diffraction pattern generated by a fluorescent particle that is found below the focal plane of an optical microscope. The particle is then tracked from the analysis of a sequence of digitized images to reconstruct its trajectory, which provides relevant information about the properties of the system. In a first stage, we obtain the mean square displacement (MSD) of a spherical probe dissolved in a viscoelastic solution. This MSD is then used to determine the elastic and viscous moduli of the suspension. Such measurements are consistent with bulk measurements performed by means of two techniques, namely, diffusing wave spectroscopy and mechanical rheology. Near the rigid wall, the motion of the probe particle can be split in two directions, *i.e.*, parallel and perpendicular to the surface. For short times (but still in the Brownian regime), such motion can be characterized by means of two distance dependent friction coefficients. We observe deviations of the measured friction coefficients in comparison with the Newtonian behavior.

Keywords: Three-dimensional digital video microscopy; Brownian motion; viscoelastic fluid.

PACS: 07.79.Lh; 82.70.Dd; 05.40.-a; 83.10.Mj

1. Introduction

The study of the mechanical properties of complex fluids has been the subject of intense research during the last two decades. Such properties are very important for industrial processes of foods, cosmetics and paints, and also for understanding the microrheology of certain biological systems. In 1995, Mason and Weitz [1] presented a new method for measuring the viscoelastic properties of fluids through the determination of the mean square displacement (MSD) $\langle \Delta r^2(t) \rangle$ of a probe particle immersed in the fluid under study. Their measurements were done by using diffusing wave spectroscopy as well as dynamic light scattering. From that moment, a variety of methods associated with such proposal have been utilized to characterize the mechanical properties of small systems like the cytoplasm of living cells [2, 3] or to describe the hydrodynamic interactions between a spherical particle and a hard wall [4] or a soft interface [5].

In this paper, we propose the use of a three-dimensional extension of video microscopy to study the MSD of a colloidal particle dispersed in polymeric solutions. In Fig. 1, we draw the main components of DVM-3D. The colloidal sample (Sample) consists of fluorescent beads suspended in aqueous solutions that contain variable concentrations of dissolved polyacrylamide at a fixed ionic strength. More important, the solute concentrations are so small that, in all cases under study, the measured refraction index (at optical frequencies) n is equal to 1.33 at room temperature. As a result, the optical path remains unchanged for all samples. An optical microscope (Olympus BX-60) is represented by an objective (Objective, in Fig. 1), which is a long working distance objective (LMPlanFl with M=100 and NA=0.8, M and

NA being the magnification and the numerical aperture, respectively). The microscope has an adapted monochromatic CCD camera (Cohu 7712 of 1004×1004 pixels with 10 bits per pixel at 30 fps) that delivers digital images to be processed and analyzed. In order to control vertical displacements with a high degree of accuracy (of a few nanometers), the objective is mounted to a piezoelectric device (Physik Instrumente E-662, LVPZT piezo amplifier/servo) whose purpose is a precise motion of the objective used to calibrate the system. Once calibrated, we compare the results of the MSD obtained through DVM-3D with equivalent measurements done with other methods. In the following section, we discuss about the preparation of the different types of samples, the calibration process as well as the validation of our technique.

2. Experimental Section

2.1. Samples preparation

We compounded polymeric solutions of polyacrylamide (Sigma) of molecular weight $M_w = 5 - 6 \times 10^6$ gr/mol. The polymeric solutions are prepared by dissolving the polyacrylamide in distilled deionized water of resistivity 18.2 MΩ·cm (Barnstead). All solutions are prepared by weight. The solutions are stirred at 40 °C for two weeks until all components are completely dissolved. Otherwise, the concentrations of our solutions are always above the known overlap concentration, *i.e.*, $c^* = 7 \times 10^{-3}$ %(w/w) [6]. It is well known that the intermolecular interactions between polyacrylamide chains are not negligible, eventually leading to viscoelastic effects and to gels at higher concentrations.
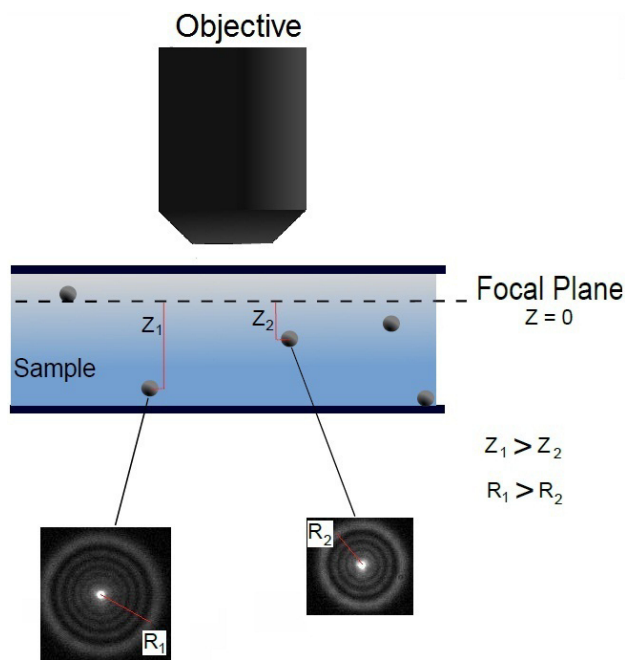
Objective

FIGURE 1. Schematic drawing of the main components of the technique DVM-3D (see text). The microscope objective is focused on a focal plane (FP) located at $Z = 0$. Fluorescent microspheres found at the distances Z_1 and Z_2 below the FP give rise to diffraction patterns characterized by an external ring of radius R_i ($i = 1, 2$). If $Z_1 > Z_2$ then $R_1 > R_2$.

In the case of video microscopy measurements, a low concentration of fluorescent polystyrene spheres of diameter 1 μm and size polydispersity of 3 % (Duke Scientific) is added to the polymeric solution. These spherical particles are only used as probes. We note that the original colloidal suspension is stabilized by charge, therefore, we add 10 mM of NaCl to screen any electrostatic interaction. The mixture is agitated to ensure homogeneity and the resulting suspension is confined between two cleaned glass plates (a slide and a cover slip). The distances between the glass plates are 600 μm and 300 μm for bulk and near wall measurements, respectively. The system is sealed with epoxy resin (Epotek) to avoid evaporation and flows. In the case of light scattering experiments, we used particles of diameter 2 μm (of same polydispersity) at a fixed volume fraction $\phi = 0.021$. The solutions are also stirred (with their corresponding electrolyte) and put in rectangular cuvettes (Hellma). The samples are allowed to equilibrate, for at least 30 min, in contact with a circulating bath at 24 °C.

2.2. Digital video microscopy in three dimensions

The polymeric solutions containing fluorescent beads are observed through the microscope under fluorescent illumination. According to the properties of the dyes that are intercalated in these beads, we use a fluorescence filter cube with the following characteristics. Excitation filter: 420-440 nm, dichromatic mirror: 455 nm, and emission filter: $\geq$ 475 nm. When a spherical fluorescent particle of about 1 μm in di-

ameter is found below the focal plan (FP), we can take advantage of its diffraction pattern to determine its depth with respect to the FP (see Fig. 1). On the other hand, if the fluorescent bead is located above the FP, its diffraction pattern can be described as a single blurry disc that provides useless information for the determination of its depth. The main idea was first introduced by Park *et al.* to perform local measurements of the temperature [7]. The microscope optics and the CCD camera actually detect a cross section of the point spread function [7, 8], which can be described by means of Kirchhoff's diffraction integral,

$$I(x_d, y_d, \Delta z) = \left(C \int_0^1 J_0 \left[k \frac{NA}{\sqrt{M^2 - NA^2}} \rho \sqrt{x_d^2 + y_d^2} \right] \right.$$

$$\left. \times \exp[iW(\Delta z, \rho)] \rho d\rho \right)^2, \tag{1}$$

here, (x_d, y_d) is the detector position, Δz is the distance to the FP (also known as defocus distance), k is the wave number, ρ is the normalized radius in the exit pupil, and $W(\Delta z, \rho)$ is a phase aberration function. It is not easy to accurately use Eq. (1), because it is difficult to estimate $W(\Delta z, \rho)$. Nonetheless, this integral predicts a finite number of concentric rings. More important, the last ring is the brightest and its size changes monotonically as a function of the separation Z_i between the sphere and the FP, as sketched in Fig. 1.

Instead of using Eq. (1), we opted to do an experimental calibration of the system that turns out to be more accurate than the results extracted from such equation. This calibration, however, is only useful for our specific optical setup (in other words, each optical system requires its own calibration). We performed a series of vertical scans by taking advantage of the piezoelectric device (eventually, it is possible to do the scan by means of the fine adjustment knob of the microscope [10]). Each scan consists of a given number of snapshots (> 100) of a fluorescent microbead that is fixed to the glass slide. The images are taken with a separation of 0.1 μm and moving in the upper direction (for the first image, the FP is placed inside the slide). Then, the digital images are analyzed with a specialized software (IDL or Matlab) that locates the center of the particle and also the external ring (when it appears). An angular jpg is done to enhance the shape of the rings. We define the radius R of the last ring as the position of its local maximum intensity (see the inset of Fig. 2). In order to accurately determine such position, we fit about 12 surrounding points with a Gaussian function. In Fig. 2, we plot the experimental radius R as a function of the distance Z, which is the separation between the center of the sphere and the FP. The experimental curve is properly fit with an exponential function of the form $R = a_1 \exp[a_2 Z] + a_3$, with a_1, a_2, and a_3 being fitting constants. We should mention that we actually require the distance Z as a function of R to determine Brownian trajectories, therefore, we use the inverse function $Z = \ln[(R - a_3)/a_1]/a_2$ in our algorithms.
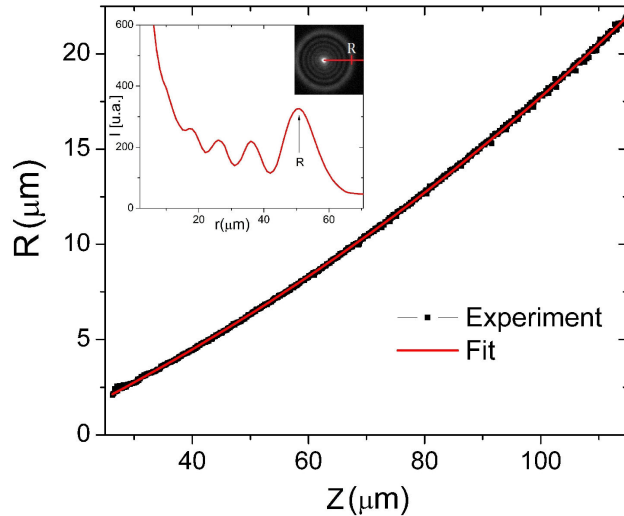
FIGURE 2. The angular averaged diffraction pattern is plotted in the inset, where the radius R of the external ring is defined as the position of the last maximum. The experimental measurements of R are plotted as a function of the separation Z between the center of the particle and the FP. An exponential fit to the experimental data is also shown.

In order to estimate the uncertainty of the measured coordinates, we captured some image sequences of particles that are fixed to the glass wall and we averaged their positions, which resulted slightly different between them due to fluctuations in the detection system. Accordingly, we obtained the following standard deviations, $\Delta X = \Delta Y = 0.015 \ \mu m$ and $\Delta Z = 0.09 \ \mu m$. A larger uncertainty in the vertical direction is a consequence of the indirect procedure used to determine the Z coordinate. These three standard deviations together with the frame separation of 1/30 s impose the lower limits in space and time of the technique. For certain properties, like the MSD, the contribution of ΔZ can be easily removed since it is not originated by a diffusion process (*e.g.*, see Sec. 3.2). On the other hand, the upper space limit is estimated at about 100 μm and the long times are only limited by the RAM capacity of the acquisition computer. In our case, we analyzed series of 2000 images. Once having the Cartesian coordinates of a colloidal particle, we can obtain its trajectory from a sequence of images. A comparison with the results of known techniques is first envisaged.

2.3. Diffusing wave spectroscopy

In order to test DVM-3D, we utilized a multiple scattering technique known as diffusing wave spectroscopy (DWS) that consists of a laser beam striking a slab formed by an opaque sample. The sample contains the polymeric solution under study and also a high concentration of probe particles (uniform spheres). The particle motion is studied over length scales shorter than the wavelength of the laser (514.5 nm, in our case). The photons inside the sample are treated as random walkers, meanwhile, the transport of light through the slab is studied as a diffusive process.

The diffusion approximation is valid over distances longer than the transport mean free path l^*. The way we detect the intensity of single speckle spots of the scattered light is very similar to the case of dynamic light scattering (DLS). Such measurements allow us to determine time correlation functions. Within this approximation, a total correlation function is obtained by summing over the contributions of all paths that are weighted with the appropriate distribution of paths as a function of the slab's geometry. We use an optical arrangement for DWS in transmission geometry, as shown in Ref. [11]. The intensity autocorrelation function $g^{(2)}(t) = \langle I(t)I(0) \rangle / \langle I(0) \rangle^2$ is determined by measuring the scattered light intensity. On the other hand, the field autocorrelation function $g^{(1)}(t) = \langle E(t)E^*(0) \rangle / \langle E(0) \rangle^2$ is related to $g^{(2)}(t)$ through the Siegert relation $g^{(2)}(t) = 1 + \beta |g^{(1)}(t)|^2$, where the parameter β is an instrumental factor obtained by collection optics.

During the measurement, the spherical probes are free to move around the same local region of the fluid, therefore, we can assume that the scattering process is diffusive. In the transmission geometry, the thickness of the slab is $L \gg l^*$. Once the light strikes the slab, it travels a distance $\sim l^*$. After that, its propagation direction is randomized. The expression of time averaged field correlation function $g^{(1)}(t)$ has an exact form for this particular geometry [9],

$$g^{(1)}(t) = \frac{\frac{L/l^* + 4/3}{\delta^* + 2/3} \left(\sinh[\delta^* x] + \frac{2}{3} x \cosh[\delta^* x] \right)}{\left(1 + \frac{4}{9} x^2 \right) \sinh\left[\frac{L}{l^*} x \right] + \frac{4}{3} x \cosh\left[\frac{L}{l^*} x \right]}, \quad (2)$$

where $x = \left[k^2 \langle \Delta r^2(t) \rangle \right]^{1/2}$ and $\delta^* = z_0/l^*$, with z_0 being the distance into the sample from the incident surface to the place where the diffuse source is found. We have a dependence in the MSD $\langle \Delta r^2(t) \rangle$ of the probe particles that can be obtained by using a numerical inversion from Eq. (2). We utilized a home-made instrument for DWS and a slab of thickness $L = 2.5$ mm [11]. The transport mean free path of light l^* of the sample is measured by means of an integrating sphere (Oriel) [12]. The mean value for our samples is $l^* = 270$ nm.

3. Results and discussion

We performed measurements of the MSD in the bulk and also near a wall by means of the techniques described in the previous sections.

3.1. Bulk properties

The MSD $\langle \Delta r^2(t) \rangle$ of an isolated particle provides interesting information about the diffusion of such probe through a given fluid. If the fluid has a Newtonian behavior, $\langle \Delta r^2(t) \rangle \sim D_0 t$, which is Einstein's celebrated result [13], where $D_0 = k_B T/\xi_0$ is the Stokes-Einstein diffusion coefficient. Here, $\xi_0 = 6\pi a \eta$, a is the radius of the sphere, $k_B T$ is the thermal energy, and η is the shear viscosity of the solvent. On the other hand, the treatment of a viscoelastic fluid

requires the use of a generalized approach that can be characterized by a complex shear modulus $G^*(\omega)$ with ω being a frequency of shearing. The real part $G'(\omega)$ is called the elastic storage modulus, whereas, the imaginary part of $G''(\omega)$ is known as the viscous loss modulus. Both moduli satisfy the Kramers-Kronig relations and can be expressed as [14],

$$G'(\omega) = G(\omega)\cos[\pi\alpha(\omega)/2],$$
$$G''(\omega) = G(\omega)\sin[\pi\alpha(\omega)/2], \tag{3}$$

with

$$G(\omega) = \frac{k_{\rm B}T}{\pi a\langle \Delta r^2(1/\omega)\rangle\Gamma[1+\alpha(\omega)]}, \tag{4}$$

here, $\langle\Delta r^2(1/\omega)\rangle$ is the magnitude of $\langle\Delta r^2(t)\rangle$ evaluated at $t = 1/\omega$, Γ is the gamma function, and $\alpha(\omega) = [\partial\ln\langle\Delta r^2(t)\rangle/\partial\ln t]|_{t=1/\omega}$.

In regard to the experimental comparison of both techniques, in Fig. 3 we present measurements of $\langle\Delta r^2(t)\rangle a$ for polyacrylamide in aqueous solutions at the polymer concentrations of 0.2 % and 0.5 %. Both curves were obtained from the average of 150 and 104 trajectories, respectively. First, we should mention that the MSD is multiplied by the radius a to remove the dependence on the size of the probe particle. Although both techniques cover different time scales, the curves of DWS and DVM-3D are consistent for the two systems under study, as it can be noted in such figure. In a more stringent test for DVM-3D, in Fig. 4 we plot the moduli $G'(\omega)$ and $G''(\omega)$ that are derived from the MSDs of the two approaches under study, through Eqs. (3) and (4). Moreover, in the same Fig. we include the results determined by using mechanical rheology for both moduli [16]. In this case, the polyacrylamide concentration is 0.5 %. As it can be noticed, the curves obtained within DVM-3D and mechanical rheology are in reasonable agreement for the two moduli.
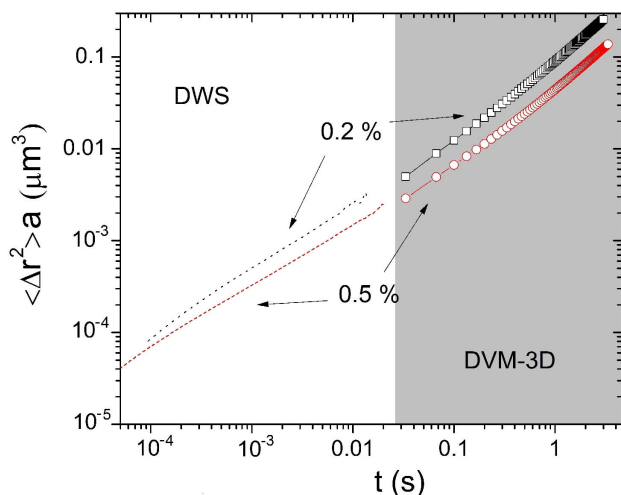

FIGURE 3. Mean square displacement (MSD) multiplied by the radius of the sphere measured by means of two techniques, namely, DWS and DVM-3D (see text). The systems under study are aqueous solutions of polyacrylamide at the polymer concentrations of 0.2 % and 0.5%.
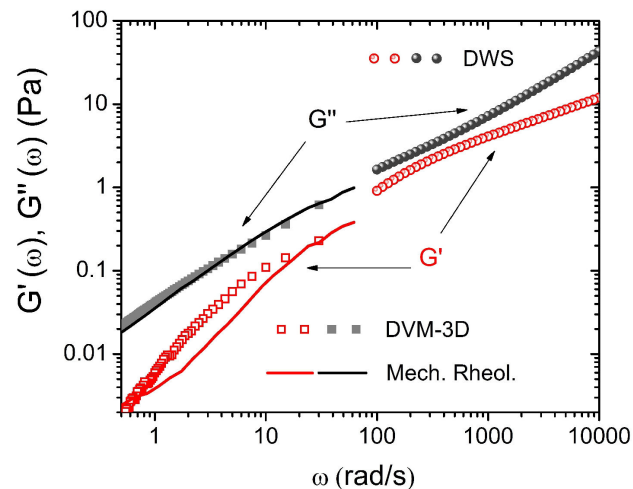

FIGURE 4. Elastic and viscous moduli $G'(\omega)$ and $G''(\omega)$ obtained for the polyacrylamide solution of 0.5 %. The experiments were performed with three techniques, *i.e.*, DWS (circles), mechanical rheology (continuous lines), and DVM-3D (squares).

This kind of agreement is usually found in the literature when similar systems to ours are studied with different techniques [15]. Furthermore, the results determined through DWS of $G'(\omega)$ and $G''(\omega)$ provide an extension, in the frequency domain, of the two moduli. In the same figure, it can be observed that the viscous behavior predominates over the elastic response, in other words $G''(\omega) > G'(\omega)$, which is expected due the low polymer concentration of the solution under analysis.

Otherwise, we can mention that both DWS and DVM-3D have advantages and shortcomings with respect to the other one. For example, the frequency range that can be studied within DWS (from 10^2 to 2×10^4 rad/s) is considerably higher than the covered range of DVM-3D (*i.e.*, from 0.3 to 30 rad/s). In the first system, the scattered light is collected by photomultiplier tubes (Thorn EMI) and the signals are processed in a multitau correlator (ALV), which is able to solve higher frequencies than the scanning frequency of our CCD device. Additionally, DWS is useful to describe turbid liquids, while DVM-3D requires the use of transparent samples. On the other hand, DWS provides bulk properties, in contrast to DVM-3D that can also be used to study specific regions of the sample, as explained in the next subsection.

3.2. Diffusion near a rigid a wall

We are interested in describing the Brownian motion of a microsphere immersed in an aqueous solution of 0.2 % polyacrylamide and moving near a glass wall. As illustrated in Fig. 5, the movement of the particle can be split in two directions, namely, parallel and perpendicular to the wall that are characterized by their corresponding diffusion coefficients $D_\parallel(h)$ and $D_\perp(h)$, both depending on the distance h between the center of the sphere and the hard surface. In the same figure, we also represent a sphere that is fixed to the wall due to van der Waals forces and whose purpose is to reveal the exact position of the interface.
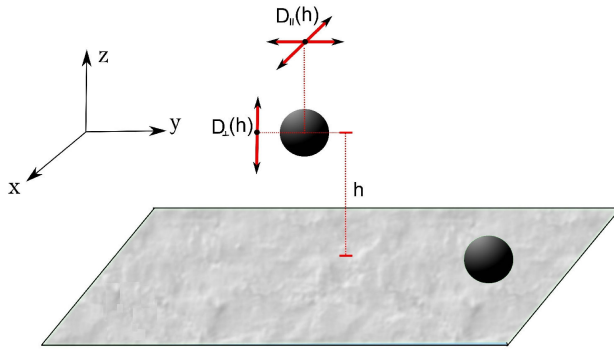
FIGURE 5. Schematic representation of the Brownian motion of a particle located near a hard interface. The movement is separated in two contributions, namely, parallel and perpendicular to the wall that are characterized by the diffusion coefficients $D_\parallel(h)$ and $D_\perp(h)$. A particle fixed to the glass wall is also represented (see text).
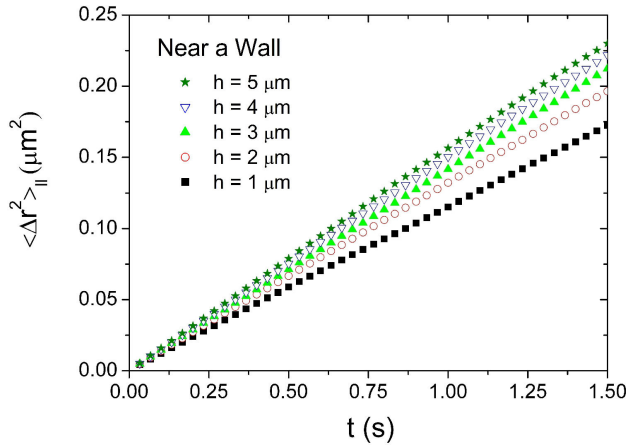

FIGURE 6. MSD in the parallel direction of a 1 μm diameter sphere immersed in a polyacrylamide solution of 0.2 %. Here, we define $\langle \Delta r^2 \rangle_\parallel = (\langle \Delta x^2 \rangle + \langle \Delta y^2 \rangle)/2$. The MSD curves are plotted as a function of time for five different separations to the wall ($h = 1, 2, 3, 4,$ and 5 μm).

We study both the parallel and the perpendicular diffusion of the sphere. In other respects, the following analysis emerges from the average of 350 trajectories. In Fig. 6, we plot the MSD as a function of five different values of h. As it can be observed, the Brownian motion is progressively restricted as the particle gets closer to the wall. As a result, the initial slope of the MSD is smaller while h decreases. This behavior is qualitatively similar to the case addressed in Ref. [4], in which the probes were located in an identical geometry but only solubilized in pure water with 10 mM of NaCl. In such work, the authors found a quite good agreement between the experimental measurements and the theory for Newtonian fluids that states the following dependence on h [17],

$$\frac{\xi_\parallel(h)}{\xi_0} = \frac{D_0}{D_\parallel(h)} = 1 - \frac{8}{15}\ln(1-\gamma)$$

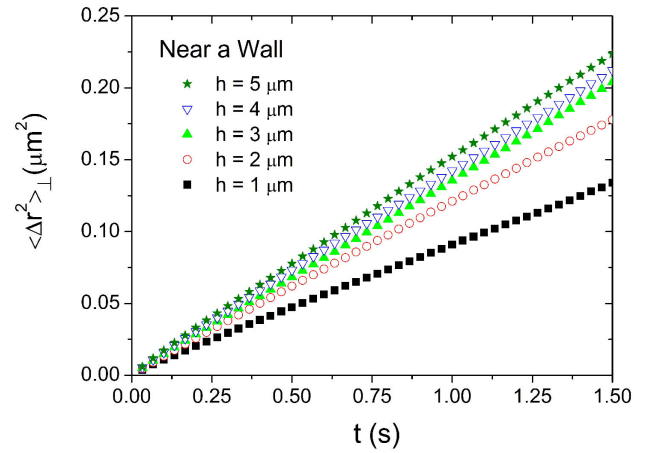$$+ 0.029\gamma + 0.04973\gamma^2 - 0.1249\gamma^3 + \cdots, \quad (5)$$

FIGURE 7. MSD in the perpendicular direction of a spherical bead diffusing at five different distances of a rigid wall. The system has the same general features that are described in Fig. 6. In this case, $\langle \Delta r^2 \rangle_\perp = \langle \Delta z^2 \rangle$. In all cases, we have subtracted the non-negligible intercept of each curve, which is about 0.007 μm^2 (and of course, $\sqrt{0.007} \simeq \Delta Z$).
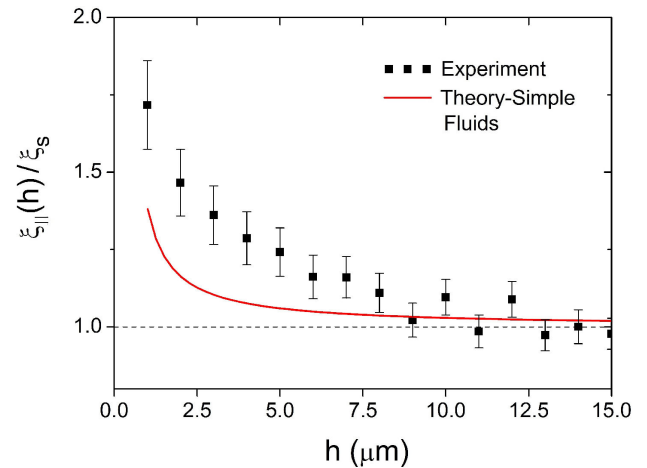

FIGURE 8. Distance dependent friction coefficient in the parallel direction that is normalized with the bulk friction coefficient $\xi_\parallel(h)/\xi_s$ determined from the experimental data of the polyacrylamide solution of 0.2 % (symbols) and the theoretical curve for a Newtonian fluid (continuous line).

here, $\xi_\parallel(h)$ is the friction coefficient in the parallel direction and $\gamma = a/h$. The corresponding expression for the friction coefficient in the perpendicular direction is [18],

$$\frac{\xi_\perp(h)}{\xi_0} = \frac{D_0}{D_\perp(h)} = \frac{4}{3}\sinh\alpha \sum_{n=1}^{\infty} \frac{n(n+1)}{(2n-1)(2n+3)}$$

$$\times \left[\frac{2\sinh(2n+1)\alpha + (2n+1)\sinh 2\alpha}{4\sinh^2(n+\frac{1}{2})\alpha - (2n+1)^2\sinh^2\alpha} - 1 \right], \quad (6)$$

where $\alpha = \cosh^{-1}(\gamma^{-1})$. With the purpose of investigating the behavior of our viscoelastic solution, we determine the initial slope of a series of MSDs that are dependent on the distance h (see Fig. 6) and we normalize the corresponding
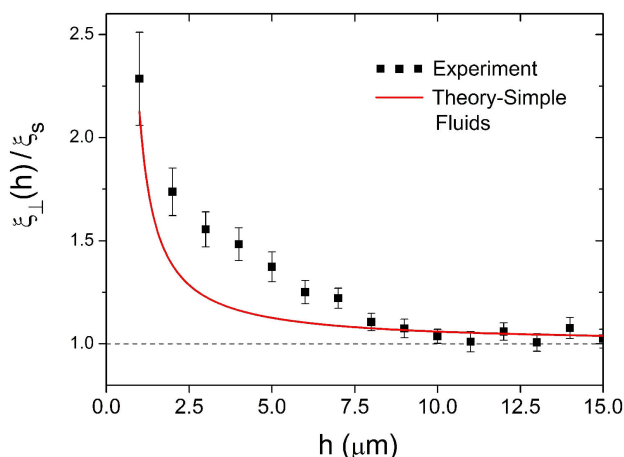
FIGURE 9. Distance dependent friction coefficient in the perpendicular direction that is normalized with the bulk friction coefficient $\xi_\perp(h)/\xi_s$. The experimental conditions are identical to those described in Fig. 8 (experimental data in symbols). The theoretical curve corresponds to the Newtonian case (continuous line).

diffusion coefficients $D_\parallel(h)$ with D_s, which is the bulk self-diffusion coefficient (of course, $D_s = D_0$ in the ideal case). In Fig. 7, we plot a series of MSDs in the perpendicular direction for the same conditions of Fig. 6. As it can be observed, the five curves are qualitatively similar to the parallel case and they allow us to determine the diffusion coefficients $D_\perp(h)/D_s$. In Figs. 8 and 9, we plot the experimental data of $\xi_\parallel(h)/\xi_s$ and $\xi_\perp(h)/\xi_s$, respectively. As a reference, we also draw the theoretical curves obtained from Eqs. (5) and (6). It can be noticed, in both figures, that there is a significant difference (*i.e.*, beyond the error bars) between Newtonian and non-Newtonian fluids. In spite of the normalization

with the bulk values, there is a considerable increment in the two friction coefficients near the wall for the viscoelastic fluid when compared to the Newtonian case.

4. Conclusions

The three-dimensional extension of video microscopy (DVM-3D) has been briefly described in some other papers [4, 5]. In the present work, we provide enough details that allow its implementation in a regular laboratory of soft condensed matter or biophysics. Moreover, we validate the results obtained from it, in comparison to the experimental data obtained through DWS, which is a well established technique. From another point of view, the information extracted from both approaches complement each other, since they cover different time intervals.

We took advantage that DVM-3D can be used in very specific regions of the sample, which could be quite interesting in the study of biological systems. In our case, we utilized DVM-3D to characterize the Brownian motion of a colloidal particle immersed in a viscoelastic fluid and located near a hard interface. As a result, we found that the friction coefficients in the parallel and perpendicular directions are enhanced by the presence of the rigid wall. As far as we know, this is an open question from the theoretical viewpoint.

Acknowledgments

1. T.G. Mason and D. A. Weitz, *Phys. Rev. Lett.* **74** (1995) 1250.

2. R.E. Mahaffy, C. K. Shih, F. C. MacKintosh, and J. Käs, *Phys. Rev. Lett.* **85** (2000) 880.

3. A. W. C. Lau, B. D. Hoffmann, A. Davies, J. C. Crocker, and T. C. Lubensky, *Phys. Rev. Lett.* **91** (2003) 198101.

4. M. D. Carbajal-Tinoco, R. Lopez-Fernandez, and J. L. Arauz-Lara, *Phys. Rev. Lett.* **99** (2007) 138303.

5. J. C. Benavides-Parra and M. D. Carbajal-Tinoco, *AIP Conf. Proc.* **1420** (2012) 128.

6. C. Haro-Pérez, E. Andablo-Reyes, P. Díaz-Leyva, and J. L. Arauz-Lara, *Phys. Rev. E* **75** (2007) 041505.

7. J. S. Park, C. K. Choi, and K. D. Kihm, *Meas. Sci. Technol.* **16** (2005) 1418.

8. S. Frisken Gibson and F. Lanni, *J. Opt. Soc. Am. A* **8** (1991) 1601.

9. D. A. Weitz and D. J. Pine in: *Dynamic Light Scattering*, W. Brown (Ed.) (Oxford University Press, New York, 1993).

10. J. C. Benavides-Parra, personal communication.

11. J. Galvan-Miyoshi, J. Delgado, and R. Castillo, *Eur. Phys. J. E* **26** (2008) 369.

12. J. Galvan-Miyoshi and R. Castillo, *Rev. Mex. Phys.* **54** (2008) 257.

13. A. Einstein, *Investigations on the Theory of the Brownian Movement.* (Dover, New York, 1956).

14. T. G. Mason, *Rheol. Acta* **39** (2000) 371.

15. T. G. Mason, K. Ganesan, J. H. van Zanten, D. Wirtz, and S. C. Kuo, *Phys. Rev. Lett.* **79** (1997) 3282.

16. The mechanical rheology data of an identical polymer solution were kindly supplied by C. Haro-Pérez.

17. G. S. Perkins and R. B. Jones, *Physica A* **189** (1992) 447.

18. J. Happel and H. Brenner, *Low Reynolds Number Hydrodynamics* (Kluwer Academic Publishers Group, Dordrecht, 1983).